Published in final edited form as:

*J Biomol NMR*. 2019 April ; 73(3-4): 191–198. doi:10.1007/s10858-019-00245-5.

# Measurement of Residual Dipolar Couplings in Methyl Groups via Carbon Detection

**Robert V. Williams**[1,2], **Jeong-Yeh Yang**[2], **Kelley W. Moremen**[2,3], **I. Jonathan Amster**[1], **James H. Prestegard**[1,2,3,*]

[1]Department of Chemistry, University of Georgia, Athens, GA

[2]Department of Biochemistry and Molecular Biology, University of Georgia, Athens GA

[3]Complex Carbohydrate Research Center, University of Georgia, Athens, GA

## Abstract

Residual dipolar couplings (RDCs) provide both structural and dynamical information useful in the characterization of biological macromolecules. While most data come from the interaction of simple pairs of directly bonded spin-1/2 nuclei ($^{1}$H-$^{15}$N, $^{1}$H-$^{13}$C, $^{1}$H-$^{1}$H), it is possible to acquire data from interactions among the multiple spins of $^{13}$C-labeled methyl groups ($^{1}H_3$-$^{13}$C). This is especially important because of the advantages that observation of $^{13}$C-labled methyl groups offers in working with very large molecules. Here we consider some of the options for measurement of methyl RDCs in large and often fully protonated proteins and arrive at a pulse sequence that exploits both J-modulation and direct detection of $^{13}$C. Its utility is illustrated by application to a fully protonated two domain fragment from the mammalian glycoprotein, Robo1, $^{13}$C-methyl-labeled in all valines.

### Keywords

Methyl Groups; $^{1}$H-$^{13}$C Methyl RDCs; Carbon Detection; Proteins; Glycoproteins

## Introduction

Isotope labeling of methyl groups simultaneously in all or a subset of isoleucine, leucine, and valine residues [1–3], or selectively in alanine[4,5] or methionine[6] residues, has emerged as a powerful method for studying large protein systems.[7,8] The improved sensitivity and resolution has been an important driver for this type of isotope labeling. Methyl proton observation is inherently more sensitive because of three equivalent protons contributing to a single signal; in addition, spin relaxation interference (methyl-TROSY effects) narrows lines, especially carbon lines in heteronuclear multiple quantum coherence (HMQC) spectra. This further improves sensitivity. However, when labeling only methyl groups, the reduced number of observable sites in a typical protein has made the collection of a more diverse set

*Corresponding author phone: jpresteg@ccrc.uga.edu; 1-706-542-6281.

Supplementary Material

Pulse sequence and parameter files for Bruker TopSpin 4.0.4.

of structural data types important. Among the data that can be collected are residual dipolar couplings (RDCs). RDCs provide information on bond vector orientation relative to the alignment frame of partially oriented molecules.[9] These can in turn be used to refine the global structure of a protein, facilitate resonance assignment, and probe domain orientation and dynamics. Interactions leading to methyl RDCs are potentially a little more complicated than those leading to the more commonly observed $^{1}H$-$^{15}N$ RDCs. Rapid methyl rotation leads to projection onto the axis of methyl rotation rather than a C-H bond and the C-H bond is slightly longer than the N-H bond, leading to a reduction by a factor of 0.27. However, this is compensated by the larger $^{13}C$ moment, resulting in RDCs that are about 70% the size of $^{1}H$-$^{15}N$ RDCs. Measurement is also a little more complex because of the increased multiplicity of coupled methyl systems. Here we introduce a method that avoids some of the complexities of dealing with methyl multiplets and yields methyl RDCs with reliable error estimates.

Measurement techniques for methyl RDCs have been developed in the past. Most rely on indirect detection in heteronuclear multiple quantum coherence (HMQC) or heteronuclear single quantum coherence (HSQC) style experiments and measurement of RDCs in a frequency domain.[10–12] Kontaxis and Bax [10] introduced a method based on a constant time (CT)-HSQC pulse sequence with spectral editing in the indirect dimension to produce 4 sub-spectra that could be combined to produce spectra containing a single component of the multiplet. More recent methods have taken advantage of the Methyl-TROSY effect in HMQC type experiments that dramatically improves resolution for large, perdeuterated proteins and protein complexes.[7,8] And, Sprangers and Kay[11] implemented an HMQC-IPAP experiment that allowed measurement of the coupling constant from the direct $^{1}H$ frequency dimension. Recently, our lab has utilized an HMQC pulse sequence that introduced J-modulation (actually J+D, where D is the RDC contribution) in the first polarization transfer element in order to extract an RDC by fitting time domain data.[12] While J-Modulation experiments require collection of multiple points in a third time domain, the number of points can be small in number and selected to optimize sensitivity to the J-modulation frequency. Also, programs used to fit the data usually provide a direct estimate of error, something that is important in using RDCs for either resonance assignment or structure refinement.

Indirect detection of a heteronucleus through attached protons, as is done in an HMQC experiment, is not always optimal. These experiments include significant periods of time where proton magnetization is transverse. For large molecules proton transverse relaxation becomes very efficient and significant intensity is lost during these periods. In these cases, the loss may actually outweigh the sensitivity advantages of proton detection. This has been nicely illustrated by the Wagner group where direct detection of $^{15}N$ in large proteins using an $^{15}N$-optimized NMR probe out performs more conventional experiments using a proton optimized probe.[13,14] This is especially the case with proteins that are not perdeuterated, as transverse proton spin relaxation becomes even more efficient and interference effects leading to TROSY enhancements are outweighed by other relaxation pathways. A similar situation occurs with $^{13}C$-methyl detection. Many of the proteins we study are glycosylated proteins that are best expressed in mammalian cell culture where perdeuteration is not an option. Hence, proton relaxation is efficient. Moreover, we frequently use the anisotropic

magnetic susceptibility of paramagnetic tags to induce the partial alignment needed for RDC measurement. This adds additional relaxation mechanisms that further enhance proton relaxation in comparison to $^{13}C$ relaxation.

Here, we propose an experiment for measuring RDCs that combines the inherent sensitivity of methyl groups with the favorable relaxation properties of carbon observation. We retain a J-modulation element due to the convenience of fitting data in the time domain and eliminate multiplet complexities from this element by making it constant time for evolution of all proton magnetization except that involving carbon. Application is to a $^{13}C$-valine-methyl labeled construct containing the two N-terminal Ig-like domains of a fully protonated glycoprotein, Robo1. The N-terminal domain has a lanthanide-binding peptide replacing a short loop between two beta strands.[15] Comparison of paramagnetic ($Dy^{3+}$ or $Tb^{3+}$) and diamagnetic ($Lu^{3+}$) complexes, as well as field dependence of the $Dy^{3+}$ complex, is used to extract RDCs. The data are expected to elucidate the inter-domain geometry of this molecule and contribute an understanding of how it may transmit signals that govern axon guidance in developing nerve cells.

## Experimental

### Isotopic Enrichment, Protein Expression and Purification.

Design, expression, and purification of the two-domain construct of Robo1 containing a lanthanide binding loop has been described elsewhere.[15] Briefly, Robo1 was expressed in *lec*$^{-}$ HEK297 cells grown in FreeStyle medium deficient in valine and supplemented with [$^{13}C$, $^{13}C$]-methyl-valine. Purified protein was treated with endoglycosidase F, leaving a single N-acetylglucosamine residue at the one glycosylation site (confirmed by mass spectrometry).

### Sample Preparation.

Solutions of the Robo1-Ig1–2-loop construct, $^{13}C$ labeled in all valine methyls, were prepared in 100% $D_2O$, 25 mM tris buffer, 100 mM KCl, 4 uM DSS, 3 uM $NaN_3$, pH 7.4 (uncorrected) at a final concentration of 300 uM. For the diamagnetic sample, an equimolar amount of lutetium chloride ($LuCl_3$) was added, while the paramagnetic samples were prepared using an equimolar amount of dysprosium chloride ($DyCl_3$) or terbium chloride ($TbCl_3$).

### NMR Spectroscopy.

Spectra were recorded on a 600 MHz magnet with a Bruker DCH probe optimized for $^{13}C$ detection and an Avance III Console or on a 900 MHz magnet with a Bruker TCO probe optimized for $^{15}N/^{13}C$ detection and an Avance III Console. J-Modulated HETCOR data were collected with 2048 x 32 points and spectral widths of 6 and 3 ppm in the direct and indirect dimensions, respectively. All spectra were processed identically using nmrPipe.[16] In the direct dimension, data were zero-filled and apodized with a cosine-bell, while in the indirect dimension the number of points was increased to 64 using linear prediction, zero-filled and apodized with a cosine-squared-bell. Peak picking was performed in Sparky,[17] and integrals were taken using nmrPipe with a footprint fixed in size and position that captured about 80% of modulated crosspeak intensity.

### Data Analysis.

J-modulation curves were extracted from the processed data and converted to text format using nmrPipe.[16] Coupling constants were extracted by curve fitting implemented in MATLAB. The curve was assumed to be of the form: $e^{(-R\tau)}\sin(\pi(J+D)2\tau - c)$, where (J+D) is the extracted coupling, $\tau$ is the variable modulation delay, R is a decay factor, and c is a phase offset associated with imperfections in the experimental setup; R, (J+D) and c are the fitting parameters.

## Results

$^{13}$C-detected two dimensional $^{1}$H-$^{13}$C spectra of our Robo1 construct (a HETCOR spectrum) are shown in Figure 1. Black crosspeaks are from a 300 μM sample with a diamagnetic ion ($Lu^{3+}$) in its lanthanide-binding loop; this spectrum was collected in approximately 3 hrs at 600 MHz for protons on a 300 μL sample. The resolution, particularly in the $^{13}$C dimension, is excellent for a fully protonated 25 kDa protein. There are 19 valines in the construct; 36 of the 38 expected peaks are observable. The sensitivity is also excellent and is very comparable to that of a spectrum collected at 600MHz with a proton optimized cryoprobe (manuscript in preparation). The red crosspeaks are from samples with a paramagnetic lanthanide ion in the binding loop ($Dy^{3+}$ in the upper panel and $Tb^{3+}$ in the lower panel). There are notable pseudo contact shifts (PCSs) in both cases. As shifts are approximately the same in both $^{1}$H and $^{13}$C dimensions, peaks in the presence of diamagnetic and paramagnetic ions can be connected by diagonal lines in most cases. The shifts are slightly different for $Dy^{3+}$ and $Tb^{3+}$ due to the different magnetic susceptibility anisotropy tensors for the two paramagnetic complexes.[18] Also, the paramagnetically shifted peaks are missing in several cases due to the enhanced relaxation. However, the loss of peaks is significantly less than in corresponding HSQC or HMQC spectra, because of the absence of an additional $^{1}$H observation period where paramagnetic contributions to transverse relaxation are larger than for $^{13}$C.

There are some subtilties to collection of the spectra in Figure 1. Transfer of proton magnetization at the end of the $t_1$ period results in antiphase components for the four proton-coupled $^{13}$C lines. A simulation in the absence of paramagnetic relaxation contributions for the spectrum at this point using MATLAB scripts that calls functions from the SPINACH package[19] is shown in Figure 2. The behavior of an isolated $^{13}C^{1}H_3$ methyl group with rapid rotation about its symmetry axis and tumbling with the correlation time of a protein was simulated by giving it an on-axis rotational correlation time of 10 ps and an off-axis correlation time of 10 ns. Note that the inner multiplet components are sharper because of the partial interference of α and β spins in the mixed proton states for these lines. The relative integrals are actually 1:1:1:1 because the experiment begins with proton magnetization and there is three times the magnetization transferred to the outer lines, compensating for the three-fold degeneracy of the inner lines. Immediate decoupling of protons would result in zero signal. Full refocusing of the $^{13}$C magnetization before decoupling is not possible but decoupling after a total refocusing delay of 1/3J results in a single line of nearly twice the intensity of the two sharper central lines with no contribution from the outer lines. A slightly shorter delay results in maximum refocusing of intensity in

the limit where all lines have equal widths.[20] Note that RDCs can in principle be measured by acquiring a coupled spectrum immediately after transfer of proton magnetization. However, turning each crosspeak of Figure 1 into the four crosspeaks of Figure 2 with a mix of positive and negative intensities would be very hard to deconvolute.

There have also been some attempts to measure RDCs directly in the proton dimension.[11] To illustrate the complexities of this approach we have simulated a $^{13}$C-coupled proton spectrum using SPINACH functions (see Figure 3). As for Figure 2, rapid methyl rotation was simulated using anisotropic diffusion. The effects of partial orientation were introduced by defining an order tensor with principal values of 2e-4, 2e-4 and −4e-4 and the z-axis parallel to the methyl rotation axis. Note that, unlike a system with just scalar coupling, which would have two single lines, the presence of proton-proton dipolar couplings produces a $^{1}$H proton spectrum with two triplets. Inner lines of the triplets are sharp due to the interference of relaxation contributions from pairs of α and β $^{1}$H spins. The outer lines of the triplet are of unequal widths due to interference with relaxation contributions from the $^{13}$C spin. Again, measurement of RDCs from the positions of six superimposed crosspeaks for each crosspeak shown in Figure 1 would be difficult. Hence, we have chosen to design a pulse sequence that yields a simple time modulation of the intensity of each crosspeak seen in Figure 1.

## Sequence design.

The sequence we generated is shown in Figure 4. It is a modification of a standard HETCOR sequence in which a constant time J-modulation period has been inserted between the end of the $^{1}$H $t_1$ evolution period and transfer to $^{13}$C by a pair of $^{1}$H and $^{13}$C 90° pulses. Making the J-modulation period, T, constant time removes modulation due to proton-proton couplings. Insertion of a 180° carbon pulse at a time τ before the end of the modulation period allows modulation due to carbon-proton couplings for times that vary from 0 to T as τ is incremented from 0 to T/2. Ideally, the value of T should be long enough to allow at least two zero crossings of the coupling evolution as points near these crossings are most sensitive to the modulation frequency ($^{1}J_{CH}+^{1}D_{CH}$ in the presence of an RDC). However, measured intensities, and signal to noise ratios, decay as $\exp(-R_2T)$ as $T$ is increased, limiting the number of zero crossings that can be accessed. In our application the constant time period, T, was set to 32 ms (4/J for J = 125 Hz) and τ was incremented from 2 to 16 ms in steps of 0.93 ms. The refocusing delays at the end of the sequence allow the antiphase lines of the $^{13}$C multiplet to come partially in phase so protons can be decoupled during observation. $\tau_R$ was set to 0.8 ms to optimize signal intensity with some sacrifice in resolution over collection of just the inner lines of the $^{13}$C multiplet.

A methyl group is an $IS_3$ spin system and is not rigorously described by the common product operator treatment used to describe experiments on $^{15}$N$^{1}$H spin pairs; however, it has been shown elsewhere[7] that the eigen basis contains a spin-1/2 manifold, and for the purposes of describing the expected J-modulation a spin pair product operator treatment is adequate. For this description we will only consider magnetization that is ultimately converted to an observable form. During the indirect evolution period the C-H coupling is refocused and $^{1}$H chemical shift evolution gives $-\cos(\omega_1 t_1)\hat{I}_y$ at time point (a) in Figure. 4.

At the end of the constant-time INEPT period this magnetization becomes $-\cos(\omega_1 t_1)\sin(\pi(J+D)2\tau)\hat{I}_z\hat{S}_x$ (Figure. 4 - point b). The final refocusing period converts most of the $I_zS_x$ coherence to $S_y$ for observation. One thing that is not included in this treatment is spin relaxation. Proton transverse relaxation effects are largely eliminated by using a constant time. However, $^{13}C$ $T_1$ relaxation dephases modulation and results in a slow exponential decay. Also, the 180° $^{13}C$ pulse that interconverts α and β states interchanges the broad and narrow components of the proton triplets seen in Figure 3, potentially resulting in a small rise of intensities at longer τ values. Both of these effects are well modeled in SPINACH simulations which do show a slight decay of the sinusoidal modulation. We model this by including an exponential term $\exp(-R\tau)$ in our fitting function. One possible effect not included in the simulation is that of a small three bond $^1H$-$^{13}C$ coupling to the second valine methyl group (~4 Hz). In the interest of generality, we have not explicitly included this in our derivation. However, its small effects are likely absorbed in the exponential fitting constant, R and phase correction, c. Hence, after Fourier transform and measurements of crosspeak integrals as a function τ, intensities, *I,* are fit to equation 1.

$$\sin(\pi(J+D)2\tau + c)\exp(-R\tau) \qquad \text{Eq. 1.}$$

## RDC Measurement.

The above discussion applies to data acquired with any means of alignment. However, our Robo1 construct contains a lanthanide ion binding loop. When paramagnetic ions like $Dy^{3+}$ and $Tb^{3+}$ are present, field induced alignment can be utilized. Valine $^{13}C^{\gamma}$–$^1H$ RDCs were measured on a fully protonated sample of our 25 kDa Robo1 construct using alignment by $Dy^{3+}$ and $Tb^{3+}$ at two magnetic field strengths, 21T for 900 MHz data and 14T for 600 MHz. Fitting of modulation data in the presence of these ions gave values for (J+D). A third measurement with the diamagnetic ion ($Lu^{3+}$) provided a measurement of J. Since we do not expect J to vary significantly from site to site or with magnetic field, the average taken from the most precise measurements (those from peaks 19 and 33) was used to evaluate J (125.8 Hz) and extract RDCs from (J+D) measurements. In the diamagnetic sample, 36 peaks were observed (Figure 1); Enhanced relaxation in the samples containing paramagnetic ions caused several peaks to become greatly attenuated or disappear entirely. Also, pseudocontact shifts caused additional overlap of peaks, preventing some measurements. Of the original 36 peaks, only 10 allowed extraction of RDCs from the $Dy^{3+}$ sample and only 13 allowed extraction of RDCs from the $Tb^{3+}$ sample. The extracted RDCs are reported in Table 1; for the $Dy^{3+}$ complex at 21T they range from approximately −3 to +6 Hz, and for the $Tb^{3+}$ complex they range from approximately 0 to 7 Hz. Figure 5 shows the modulation curves of peak 16 in the diamagnetic and paramagnetic $Dy^{3+}$ samples at 21T (900 MHz). This clearly shows the difference in modulation frequency that we attribute to an RDC.

Collection of RDCs at more than one field strength can be useful. There can be field dependent broadening of resonances due to modulation of PCSs by internal motion, making some crosspeaks broader and less intense at higher fields; the known field dependence can also be used to extract an RDC in the absence of a separate measurement of scalar couplings

or, when scalar couplings are known, compare results as an additional check on data quality. Both the induced magnetic moments and the interaction energies depend linearly on magnetic field, so RDCs depend on field squared.[21] RDCs are therefore expected to be 2.25 times as large at 21 T as 14 T. In Table 1 we have scaled up the 600 MHz RDC values and their estimated errors by this factor and entered this in columns 4 and 7 so that direct comparisons of data collected at the two field strengths can be made. Three of the 21 possible comparisons lie more than 1 Hz outside the sum of our estimated errors (peak 25 for $Dy^{3+}$and 8 and 16 for $Tb^{3+}$). All three peaks are in crowded regions of the spectrum and the curve fitting procedure may be negatively impacted by signal overlap. A more sophisticated peak fitting approach that simultaneously fits multiple peaks could improve the quality of extracted intensities in these instances. The estimated errors in many cases seem large compared to the RDCs. However, it is important to point out that in applications such as crosspeak assignment or protein domain orientation, it is the error relative to the range of RDC measurements that counts. The ratio of the average error relative to the range for $Dy^{3+}$ and $Tb^{3+}$ are 0.16 and 0.22 respectively. This precision proves to be useful for many applications.

## Discussion

The above data demonstrate J-modulation combined with $^{13}C$ detection to be a viable method of measuring $^{13}C$-methyl RDCs. These RDCs are useful both for assignment of resonances and monitoring of structural changes. For proteins such as Robo1, which is natively glycosylated and best expressed in mammalian cell culture, assignment procedures based on uniform isotopic labeling are often not an option. We have recently introduced a procedure for assignment that uses comparison of easily acquired data, such as NOEs, chemical shifts and RDCs, to predictions based on known domain structures.[12,15,22] Utilization of the RDCs collected with our $^{13}C$-detected J-modulation experiment in assignment of the valine methyl resonances of our Robo1 construct is a high priority moving forward. Once assigned, there are emerging questions about the inter-domain orientation in our two-domain construct of Robo1. The RDCs we have measured, as well as the PCSs, will be useful in assessing inter-domain geometry.

Our Robo1 construct is not a particularly large protein, but even here $^{13}C$-observe methods appear competitive with $^{1}H$-observe methods. This is in part a consequence of an inability to perdeuterate natively glycosylated systems. We anticipate that the advantages of $^{13}C$-detection methods will only increase as protein targets become larger and the number of glycosylated systems under investigation increases.

The pulse sequence and data fitting protocols presented here are likely to be refined in the future. We have already mentioned the possibility of explicitly including the effects of long-range couplings, such as that from protons of the methyl group observed to the $^{13}C$ of the second intra-residue valine methyl group, in our fitting function. For methyl labeling, this is a unique problem arising from $^{13}C$-enrichment in both the methyls of the valine we used. However, similar problems can arise with leucine, and if uniform labeling of other methyl-containing amino acids is used (uniformly labeled alanine, for example), it will arise there as

well. In the latter case, substitution of a selective pulse for the hard 180° pulse in our modulation period may eliminate the problem with long-range couplings.

We have also not collected modulation data in the most time-efficient way. First, we have picked a rather long modulation period for the purpose of showing a more complete modulation curve. In principle, two zero crossings are likely to be adequate; this corresponds to T= 2/J = 16 ms, a factor of 2 shorter than that used in our illustration. While the shorter modulation time would sacrifice some precision, we would expect a substantial increase in signal to noise of each point measured. Proton transverse relaxation is occurring during our modulation period, and based on proton line widths from HSQC spectra (not shown), we estimate T2 to be roughly 11 ms. Assuming mono-exponential decay during the J-modulation element, the signal intensity would be approximately 4 times greater with a 16 ms delay than with 32 ms delay used in our data.

Also, there is no need to collect equally incremented modulation points. Assuming that noise is constant as a function of $\tau$, the contribution a measurement at a particular $\tau$ value can make to the accuracy of $J$ (or $J+D$) should be proportional to the variation of intensity with J. This variation is given in equation 2, Where the effect on intensity as a function of transverse relaxation ($R_2$) during the total modulation period, T, is also included.

$$\frac{\partial I}{\partial J} = \pi 2\tau e^{-R_2 T} \cos[\pi J 2\tau] \quad \text{Eq. 2}$$

It is clear from equation 2 that contributions would have local maxima (or minima) at $2\tau$ = n/J (zero crossings of Figure 5, where J = 125 Hz). It is also clear that values at these points would rise linearly with $\tau$, but decrease exponentially as T was made longer to accommodate additional zero crossings. For our estimate of $R_2$ contributions would drop off rapidly after the first two zero crossings. To account for other factors, including phase offsets and decay as $\tau$ is incremented, it would be advisable to also place a few of the observation points near the first maximum and minimum of the curve and clustering the rest near the first two zero-crossings. With these improvements in mind, we expect that applications to protein systems significantly larger than our Robo1 construct should be possible.

## Conclusion

We have designed a carbon detected pulse sequence for measurement of methyl $^{1}H$-$^{13}C$ RDCs, which uses an intensity modulation scheme, and we have demonstrated this pulse sequence on a fully protonated, two-domain construct from the glycoprotein, Robo1. Our proposed design allows the efficient collection of RDCs and is broadly applicable to any system containing isotopically labeled methyl groups.

## Supplementary Material

Refer to Web version on PubMed Central for supplementary material.

## Acknowledgements

Financial support was provided by National Institutions of Health grants R01-GM033225, P41-GM103390, S10-OD021623 and T32-GM107004. We thank Professor Ilya Kuprov for his prompt response to our questions regarding implementation of the SPINACH package.

## References

1. Goto NK, Gardner KH, Mueller GA, Willis RC & Kay LE. A robust and cost-effective method for the production of Val, Leu, Ile (delta 1) methyl-protonated N-15-, C-13-, H-2-labeled proteins. Journal of Biomolecular Nmr 13, 369–374 (1999). [PubMed: 10383198]
2. Tugarinov V & Kay LE. An Isotope Labeling Strategy for Methyl TROSY Spectroscopy. Journal of Biomolecular NMR 28, 165–172 (2004). [PubMed: 14755160]
3. Lichtenecker RJ. et al. Independent valine and leucine isotope labeling in Escherichia coli protein overexpression systems. Journal of Biomolecular NMR 57, 205–209 (2013). [PubMed: 24078042]
4. Ayala I, Sounier R, Usé N, Gans P & Boisbouvier J. An efficient protocol for the complete incorporation of methyl-protonated alanine in perdeuterated protein. Journal of Biomolecular NMR 43, 111–119 (2009). [PubMed: 19115043]
5. Godoy-Ruiz R, Guo C & Tugarinov V. Alanine Methyl Groups as NMR Probes of Molecular Structure and Dynamics in High-Molecular-Weight Proteins. Journal of the American Chemical Society 132, 18340–18350 (2010). [PubMed: 21138300]
6. Fischer M. et al. Synthesis of a 13C-Methyl-Group-Labeled Methionine Precursor as a Useful Tool for Simplifying Protein Structural Analysis by NMR Spectroscopy. ChemBioChem 8, 610–612 (2007). [PubMed: 17328009]
7. Ollerenshaw JE, Tugarinov V & Kay LE. Methyl TROSY: explanation and experimental verification. Magnetic Resonance in Chemistry 41, 843–852 (2003).
8. Rosenzweig R & Kay LE. Bringing dynamic molecular machines into focus by methyl-TROSY NMR. Annu Rev Biochem 83, 291–315 (2014). [PubMed: 24905784]
9. Prestegard JH, Al-Hashimi HM & Tolman JR. NMR structures of biomolecules using field oriented media and residual dipolar couplings. Quarterly Reviews of Biophysics 33, 371–424 (2001).
10. Kontaxis G & Bax A. Multiplet component separation for measurement of methyl 13C-1H dipolar couplings in weakly aligned proteins. Journal of Biomolecular NMR 20, 77–82 (2001). [PubMed: 11430758]
11. Sprangers R & Kay LE. Probing Supramolecular Structure from Measurement of Methyl 1H–13C Residual Dipolar Couplings. Journal of the American Chemical Society 129, 12668–12669 (2007). [PubMed: 17910459]
12. Pederson K. et al. NMR characterization of HtpG, the E. coli Hsp90, using sparse labeling with 13C-methyl alanine. Journal of Biomolecular NMR 68, 225–236 (2017). [PubMed: 28653216]
13. Takeuchi K, Arthanari H, Imai M, Wagner G & Shimada I. Nitrogen-detected TROSY yields comparable sensitivity to proton-detected TROSY for non-deuterated, large proteins under physiological salt conditions. Journal of Biomolecular NMR 64, 143–151 (2016). [PubMed: 26800993]
14. Takeuchi K, Arthanari H, Shimada I & Wagner G. Nitrogen detected TROSY at high field yields high resolution and sensitivity for protein NMR. Journal of Biomolecular NMR 63, 323–331 (2015). [PubMed: 26497830]
15. Gao Q. et al. Structural Aspects of Heparan Sulfate Binding to Robo1-Ig1–2. ACS Chem Biol 11, 3106–3113 (2016). [PubMed: 27653286]
16. Delaglio F. et al. NMRPipe: A multidimensional spectral processing system based on UNIX pipes. Journal of Biomolecular NMR 6, 277–293 (1995). [PubMed: 8520220]
17. Goddard TD KD. SPARKY 3. (University of California, San Francisco, 2008).
18. Nitsche C & Otting G. Pseudocontact shifts in biomolecular NMR using paramagnetic metal tags. Progress in Nuclear Magnetic Resonance Spectroscopy 98–99, 20–49 (2017). [PubMed: 29157495]

19. Hogben HJ, Krzystyniak M, Charnock GTP, Hore PJ & Kuprov I. Spinach – A software library for simulation of spin dynamics in large spin systems. Journal of Magnetic Resonance 208, 179–194 (2011). [PubMed: 21169043]

20. Keeler J. Understanding NMR Spectroscopy, (Wiley, West Sussex, UK, 2010).

21. Bertini I, Luchinat C, Parigi G & Pierattelli R. NMR Spectroscopy of Paramagnetic Metalloproteins. ChemBioChem 6, 1536–1549 (2005). [PubMed: 16094696]

22. Gao Q, Chalmers GR, Moremen KW & Prestegard JH. NMR assignments of sparsely labeled proteins using a genetic algorithm. Journal of Biomolecular NMR 67, 283–294 (2017). [PubMed: 28289927]

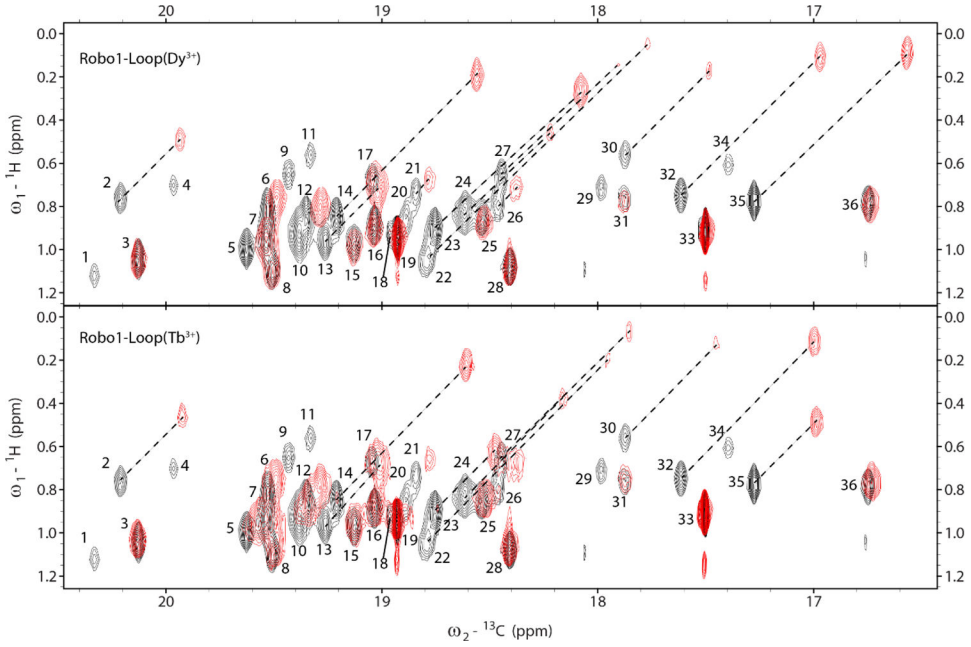


**Figure 1.**

HETCOR spectra of [$^{13}CH_3$,$^{13}CH_3$]-Valine-Robo1-Ig1–2-Loop showing overlays of the diamagnetic (black) $Lu^{3+}$ complex with the paramagnetic (red) $Dy^{3+}$ and $Tb^{3+}$ complexes. Spectra were acquired on 300 μM samples in approximately 3 hrs at 600 MHz for protons. Resonance assignments have not been completed and peaks in the diamagnetic spectra are labeled with arbitrary numbers. Several peaks experience large pseudocontact shifts in the paramagnetic spectra and are connected to their diamagnetic counterparts with dashed lines.

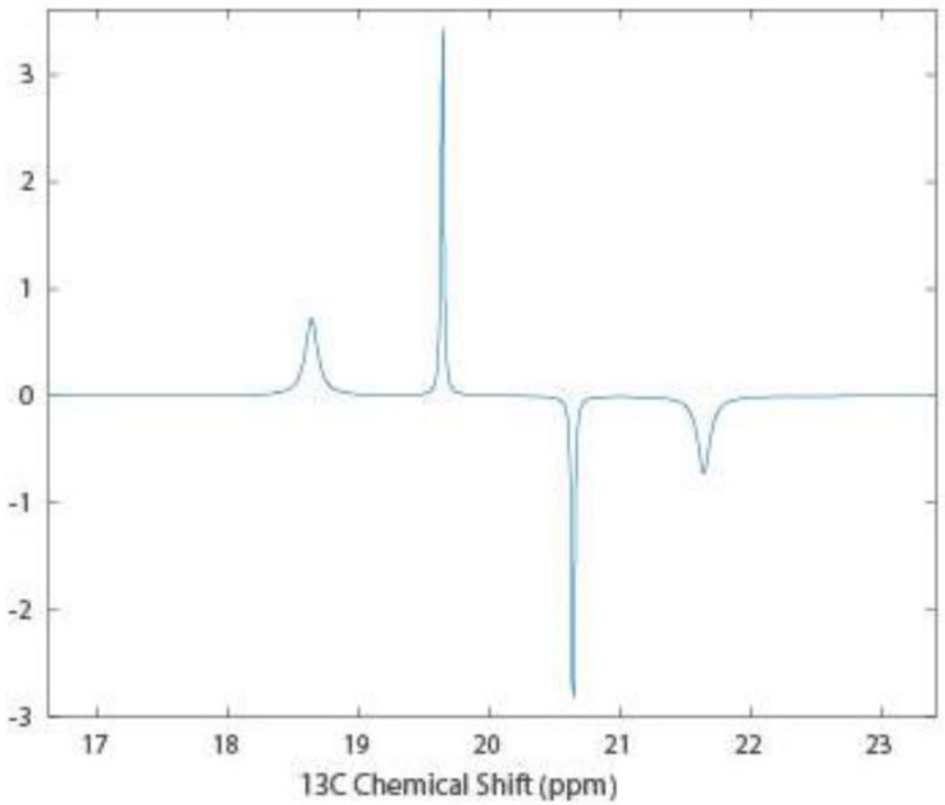


**Figure 2.**
SPINACH simulation of $^{13}C$ magnetization for a proton coupled methyl group in a HETCOR experiment before the final refocusing period.

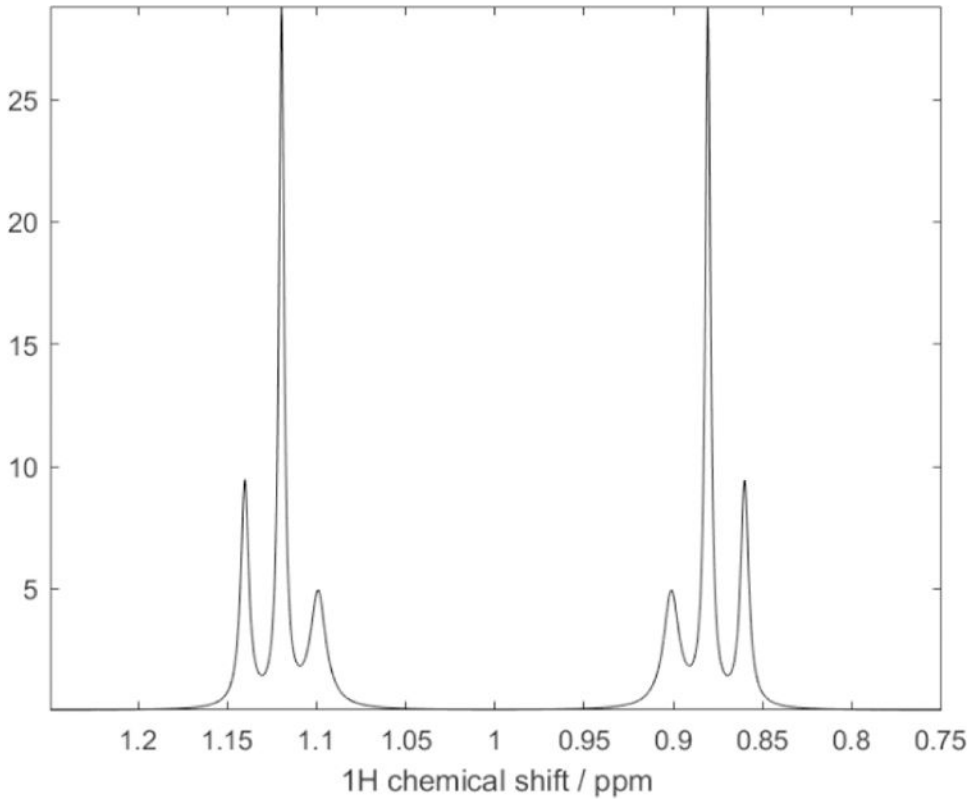


**Figure 3.**

SPINACH simulation of a 1D 600 MHz $^{1}$H spectrum of an isolated ($^{13}C^{1}H_3$) spin system under conditions of partial alignment. The large splitting is due to $^{1}J_{CH}$. The proton lines are also split into triplets due to the a $^{1}H^{-1}H$ RDC of approximately 12 Hz. Cross-correlation effects between $^{13}C$-$^{1}H$ and $^{1}H$-$^{1}H$ dipole-dipole relaxation cause the differential linewidths for the inner and outer lines of each triplet.

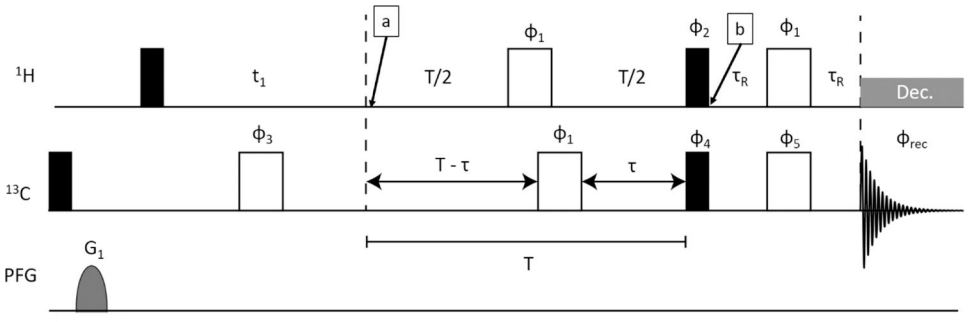


**Figure 4.**

J modulated HETCOR pulse sequence. Filled pulses are 90° and unfilled are 180°. Pulse phases are as follows: $\phi_1$ = [x, x,−x,−x], $\phi$2 = [y,−y], $\phi_3$ = [y, y, −y, −y], $\phi$4 = [4x,4y,4(−x), 4(−y)], $\phi_{rec}$ = [2(x, −x), 2(y, −y), 2(−x, x), 2(−y, y)]. All other pulses have x-phase. All gradients were 1 ms duration and strength of 52 G/cm.

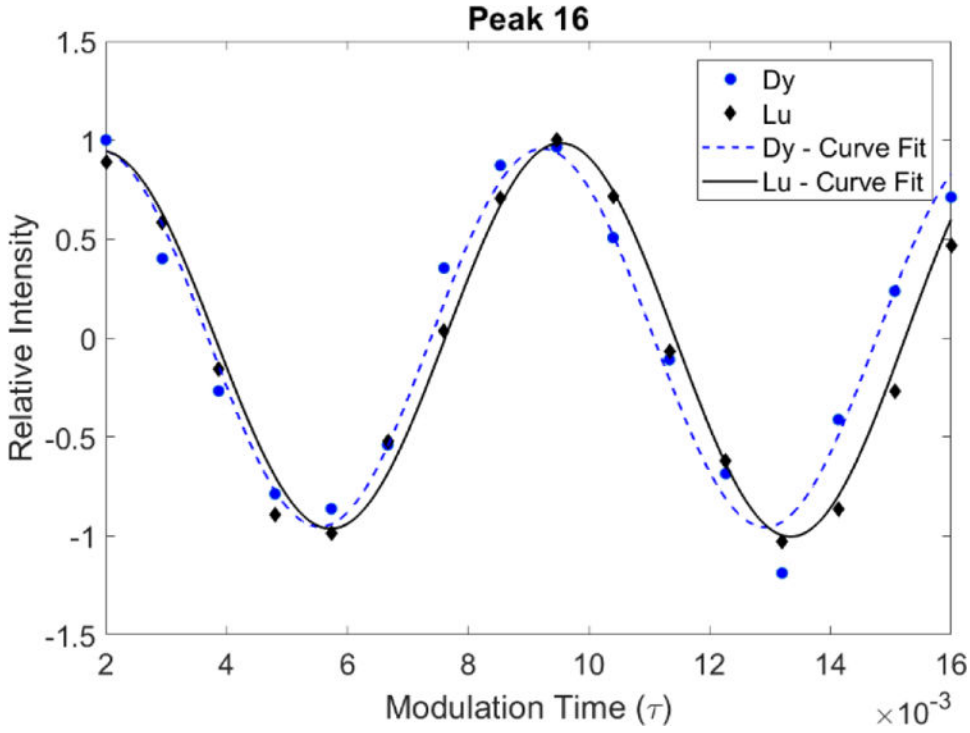


**Figure 5.**

Overlay of measured J-modulation curves as a function of **τ** for peak 16 in paramagnetic Robo1+Dy sample and diamagnetic Robo1+Lu sample recorded using the pulse sequence in Figure 4. Both samples were measured at 900 MHz at concentrations of 300μM in approximately 24 hrs.

**Table 1.**

Field-induced RDCs measured for the Robo1 $Dy^{3+}$ and $Tb^{3+}$ complexes at 900 MHz and 600 MHz. RDCs were measured as the difference in J+D in the paramagnetic complex and an average value of J from the diamagnetic complex

| | $Dy^{3+}$ Complex | | | $Tb^{3+}$ Complex | | |
|---|---|---|---|---|---|---|
| **Peak Label** | **$^{900}$DCH** | **$^{600}$DCH** | **Scaled** | **$^{900}$DCH** | **$^{600}$DCH** | **Scaled** |
| 3 | −1.8 ± 1.3 | 1.4 ± 1.8 | 3.1 ± 3.6 | 1.4 ± 1.3 | 0.2± 1.9 | 0.4 ± 2.8 |
| 5 | N/A[a] | N/A[a] | N/A[a] | 1.8 ± 1.8 | 0.8 ± 2.3 | 1.8 ± 3.4 |
| 6 | 0.1 ± 1.6 | 1.1 ± 1.5 | 2.5 ± 2.3 | −0.3 ± 1.6 | 3.5 ± 2.3 | 7.9 ± 3.4 |
| 8 | 2.1 ± 1.8 | 1.1 ± 1.9 | 2.5 ± 2.3 | 5.4 ± 1.3 | 3.9 ± 0.9 | 8.8 ± 1.4 |
| 10 | N/A[b] | N/A[b] | N/A[b] | 6.4 ± 1.7 | N/A[b] | N/A[b] |
| 12 | 6.2 ± 3.4 | 0.8 ± 2.5 | 1.8 ± 3.8 | 2.6 ± 1.8 | N/A[b] | N/A[b] |
| 15 | N/A[a] | N/A[a] | N/A[a] | 4.1 ± 2.3 | 3.5 ± 1.6 | 7.9 ± 2.4 |
| 16 | 6.4 ± 1.6 | 3.5 ± 1.4 | 7.9 ± 2.0 | 7.1 ± 2.4 | 6.1 ± 1.6 | 13.7 ± 2.5 |
| 19 | 0.0 ± 0.1 | −0.1 ± 0.2 | −0.2 ± 0.3 | −0.2 ± 0.2 | 0.2 ± 0.6 | 0.4 ± 0.8 |
| 25 | −2.7 ± 1.8 | 2.2 ± 1.4 | 4.9 ± 2.0 | 2.0 ± 3.2 | 0.6 ± 2.6 | 1.3 ± 3.7 |
| 28 | 3.9 ± 1.1 | 2.5 ± 1.5 | 5.6 ± 2.3 | 4.4 ± 0.8 | 2.9 ± 1.6 | 6.5 ± 2.3 |
| 33 | 0.0 ± 0.1 | 0.0 ± 0.3 | 0.0 ± 0.4 | −0.2 ± 0.1 | −0.3 ± 0.2 | −0.7 ± 0.3 |
| 36 | 2.7 ± 2.3 | 1.7 ± 2.5 | 3.8 ± 3.7 | 1.4 ± 2.1 | −1.2 ± 2.4 | −2.7 ± 3.5 |

[a]Peaks were greatly attenuated and reliable measurements could not be made.

[b]Peaks 10and 12 show significant overlap and could not be fit well in all spectra.. Errors are standard deviations propagated from curve fitting estimates.